Open Archive Toulouse Archive Ouverte (OATAO)

The influence of artificial ageing on the corrosion behaviour of a 2050 aluminium–copper–lithium alloy

Vincent Proton [a], Joël Alexis [b], Eric Andrieu [a], Jérôme Delfosse [c], Alexis Deschamps [d], Frédéric De Geuser [d], Marie-Christine Lafont [a], Christine Blanc [a,*]

[a] Université de Toulouse, CIRIMAT, UPS/CNRS/INPT, 4 Allée Emile Monso, BP 44362, 31030 Toulouse Cedex 04, France
[b] Université de Toulouse, LGP, ENIT/INPT, 47 Avenue d'Azereix, BP 1629, 65016 Tarbes Cedex, France
[c] EADS Innovation Works-IW/MS/MM, 12 Rue Pasteur, BP 76, 92152 Suresnes Cedex, France
[d] SIMAP, INP Grenoble-CNRS-UJF, BP 75, 38402 St. Martin d'Hères Cedex, France

ABSTRACT

The influence of artificial ageing on the corrosion behaviour of the recently developed 2050 Al–Cu–Li aluminium alloy in chloride-containing solutions was studied. Corrosion tests showed that artificial ageing changed the corrosion morphology of the alloy from intergranular to intragranular and decreased the corrosion potential of the alloy. Transmission electron microscopy observations combined with small-angle X-ray scattering measurements were used to establish a link between the distribution of T_1 precipitates and the corrosion behaviour.

1. Introduction

Reducing the weight of aircraft metallic structures is a current challenge for the aeronautic industry. Due to the increased use of composite materials, the aluminium industry has developed a new generation of aluminium–copper–lithium alloys as an alternative solution. The addition of 1 wt% lithium has been shown to induce a 3% decrease in the density and a 6% increase in the Young modulus [1]. Therefore, the replacement of 7xxx alloys in aircraft metallic structures by Al–Cu–Li alloys, which have similar mechanical properties [2], could induce a 6% reduction in weight. Further weight reductions could be achieved if the additional benefits of these alloys such as increased damage tolerance are properly considered.

Al-Cu-Li alloys are precipitation-hardening alloys; the main strengthening phases can be T_1 (of nominal composition Al_2CuLi), those of the θ' sequence (with its metastable precursors) (Al_2Cu), T_2 (Al_5Li_3Cu), T_B (Al_7Cu_4Li), S (Al_2CuMg) and δ' (Al_3Li). Other slow diffusing elements are added to these alloys to form dispersoid particles such as Al_3Zr and $Al_{20}Cu_2Mn_3$, which are helpful in controlling the grain size during homogenisation and hot rolling [3]. The competition between these different phases is closely linked to the lithium and copper content, minor solute element content [4,5] and the thermomechanical history of the alloy. Cassada et al. [6] studied the nucleation mechanism of T_1 precipitates and proposed that T_1 particles nucleate preferentially on dislocations and at sub-grain boundaries. In another study [7], they showed that plastic deformation before ageing promoted T_1 nucleation. This result was confirmed by Gable et al. [8], who found that plastic deformation before ageing at 160 °C promoted T_1 nucleation at the expense of the aforementioned precipitates. Chen and Bhat [9] proposed a time temperature precipitation diagram for 2195 Al–Cu–Li alloys and showed the predominance of T_B precipitates at high temperatures. Therefore, the mechanical properties of such alloys can be optimised by adjusting the thermomechanical treatment [10].

However, the electrochemical behaviour of these precipitate phases differs from that of the matrix; therefore, their presence in the alloy can have a significant effect on the corrosion behaviour of Al–Cu–Li alloys. The corrosion behaviour of T_1 precipitates has been widely studied in sodium chloride solutions [11–13]. These studies showed that the T_1 precipitates have a more negative corrosion potential than the matrix and were associated with dissolution phenomena such as intergranular corrosion when they were present at grain boundaries [14]. Thus, the thermomechanical treatments applied to these alloys influence the corrosion behaviour by altering the precipitate microstructure. Henon and Rouault

* Corresponding author. Tel.: +33 (0)5 34 32 34 07; fax: +33 (0)5 34 32 34 98.
E-mail address: christine.blanc@ensiacet.fr (C. Blanc).

studied the corrosion behaviour of 2050 alloy as a function of tempering and showed a susceptibility to corrosion in underaged conditions, desensitization near peak age and re-sensitization in overaged conditions [15]. The susceptibility to exfoliation corrosion of an Al–Cu–Li alloy in two different metallurgical states (T6 and T8, *i.e.*, peak aged, with and without predeformation) was studied by Li et al. [16]. When the alloy was in T6 state, it presented great susceptibility to exfoliation corrosion, whereas susceptibility was more limited in its T8 state (predeformed). The authors attributed the exfoliation susceptibility of the T6 state to the presence of a large amount of coarse T_1 precipitates at grains boundaries. Kertz et al. [17] demonstrated that the corrosion morphology of an Al 2.69% Cu 1.8% Li alloy was modified by an ageing treatment. At temperatures greater than 450 °C, the alloy was only susceptible to pitting. However, between 300 °C and 400 °C, the alloy was susceptible to both intergranular and pitting corrosion. Lastly, at lower temperatures, a long ageing treatment was necessary to sensitise the alloy to intergranular corrosion. The authors attributed the modification of the corrosion morphology to the presence of T_1 precipitates at grain boundaries and to the width of the precipitate-free zone (PFZ). Moran et al. [18] studied the exfoliation susceptibility of a 2199 (Al 2.3 wt% Cu 1.4 wt% Li) alloy using various accelerated corrosion tests. Considering that the alloy was exposed to the seacoast for 4 years, the T3 state (no artificial ageing) and the T8 state (peak aged with predeformation) presented good resistance to corrosion, whereas the intermediate metallurgical states were more susceptible to exfoliation corrosion. Moreover, other studies showed that an ageing treatment not only affected the corrosion susceptibility and morphology but also the corrosion kinetics. Jiang et al. [19] measured the average and maximal depths of the corrosion damage in an Al–Cu–Li alloy and found that these two parameters increased with an increase in the ageing time and temperature. The authors explained this phenomenon by considering that an increase in the ageing time or temperature led to an increase in the size of the T_1 precipitates and affected the precipitate-free zone (PFZ).

In summary, the existing literature shows that the corrosion behaviour of Al–Cu–Li alloys is closely linked to the distribution of T_1 precipitates. However, a definitive relationship between the distribution of T_1 precipitates and the corrosion behaviour has not been determined. To establish such a relationship, one should consider different T_1 microstructures by varying the thermo-mechanical treatments without altering the other characteristic features of the microstructure, such as the grain size, internal stresses of solute segregation to grain boundaries, because these modifications are known to influence the corrosion rate [20–25].

In the present work, we performed a detailed study on the corrosion behaviour of 2050 alloy samples after different ageing treatments and varied the intra- and inter-granular precipitate distribution. Moreover, we related the observed corrosion morphology and kinetics to a systematic characterisation of the precipitates. In parallel to the corrosion morphology observations, the corrosion kinetics in a chloride containing solution was evaluated by obtaining cross-section and residual strength measurements. The global electrochemical behaviour was evaluated using current–potential curves and open circuit potential measurements. The precipitate microstructure was characterised by combining transmission electron microscopy observations and small-angle X-ray scattering measurements.

2. Experimental

2.1. Material

The material studied in the present work was a recently developed aluminium–copper–lithium AA 2050 alloy (Al base, 3.5% Cu, 1% Li, weight percentage) provided by Constellium (France). The material consisted of 20-mm thick rolled plates of the T34 metallurgical state, which was solution treated, stretched and naturally aged. To study the influence of ageing treatments on the corrosion behaviour of AA 2050, samples were aged at 155 °C for 30 h at a heating ramp of 20 °C/h. In the following text, samples in the T34 metallurgical state and aged samples are referred to as NHT (non-heat treated) and HT (heat-treated), respectively. For some experiments, intermediate ageing times at 155 °C were also investigated (1, 2, 3, 5, 9 and 18 h). The grain structure was studied by analysing the optical micrographs on an Olympus PMG3 after etching with Keller's solution (1 mL of hydrofluoric acid 40 wt%, 1.5 mL of hydrochloric acid 35 wt%, 2.5 mL of nitric acid 68 wt% and 95 mL of distilled water). Table 1 provides a summary of the grain information. For all of the samples, the grains were elongated in the rolling (longitudinal) direction. Their mean size, which was measured in the three characteristic planes of the plate, was identical, regardless of the ageing treatment.

2.2. Study of the corrosion behaviour

All of the corrosion tests were performed in 0.7 M NaCl, which was prepared by dissolving Normapur chemical salts in distilled water. The solution was stirred and opened to air, and the temperature was maintained at 25 °C using a Julabo refrigerated circulator. The corrosion behaviour of the samples was studied using conventional immersion tests and stationary electrochemical techniques. For immersion tests, the longitudinal – longitudinal transverse (L-LT) plane of 1 cm-ridge cubic samples was exposed to the electrolyte, while the other planes were protected with a varnish. After immersion, the samples were cleaned with ethanol and dried. The samples were used to characterise the corrosion damage (Fig. 1a, the procedure is provided later in this section). Tensile samples were also submitted to immersion tests (Fig. 1b). The surface exposed to the electrolyte was the L-LT plane, which corresponded to the gauge length and a width of 5 mm. The edges corresponding to the other planes were masked with a varnish. After the immersion test, the samples were cleaned with ethanol, dried and submitted to a tensile test to evaluate the change in the mechanical properties due to corrosion damage and to evaluate the propagation depth of the corrosion damage [26]. For the electrochemical measurements, a three-electrode electrochemical cell was used, including a platinum grid with a large surface area as the auxiliary electrode and a saturated calomel electrode (SCE) as the reference electrode. All of the potentials quoted in the manuscript are with respect to the SCE reference. The working electrode corresponded to one of the previously described samples. The surface exposed to the electrolyte was the L – LT plane and possessed a surface area of 0.785 cm^2 (1-cm diameter disk). Open circuit potential (OCP) measurements were performed for approximately 2 h. The OCP values corresponded to average values calculated during the last 15 min of the test. Current–potential curves were also plotted. The anodic and cathodic parts of the curves were plotted separately. For the anodic part, the sample was maintained for 5 min at OCP; then the potential was switched to OCP – 5 mV and immediately scanned to −300 mV/SCE. For the cathodic part, the sample was maintained for 5 min at OCP; then the potential

Table 1
Grain size in the three characteristic directions of the rolled plate for the 2050-T34 (NHT) aluminium alloy: longitudinal (L), longitudinal-transverse (LT) and short-transverse (ST).

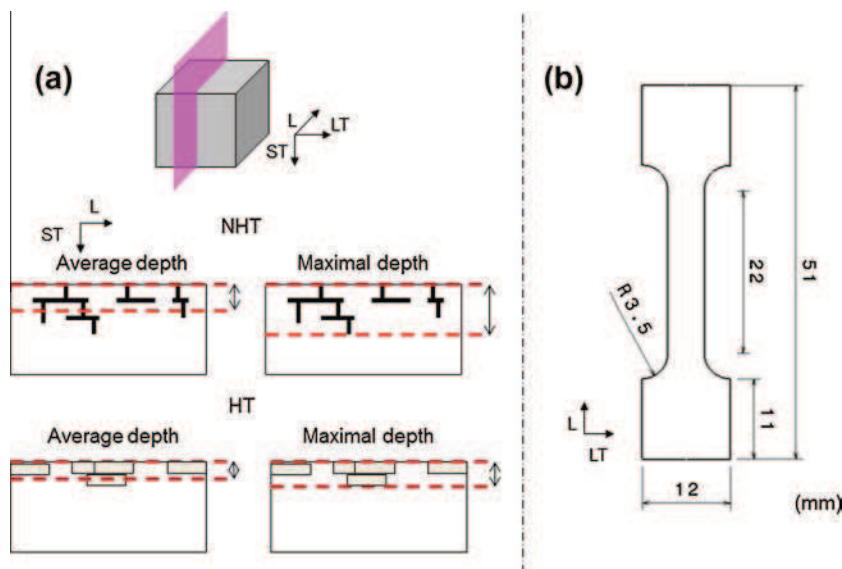| Direction	L	LT	ST
Grain size (µm)	620 ± 60	310 ± 45	40 ± 20

Fig. 1. (a) Preparation of cubic samples and a schematic diagram of the procedure established to estimate the corrosion damage. (b) The geometry of the tensile samples.

was switched to OCP + 5 mV and immediately scanned to −1000 mV/SCE. The scan rate was 500 mV h^{-1}. To check the reproducibility of the measurements and to ensure their relevancy, all electrochemical measurements (OCP and current–potential curves) were repeated at least three times. Furthermore, to avoid any problems linked to a gradient in the grain size or morphology in the 20-mm thick plate, a procedure was established to machine the samples. For all of the corrosion tests, the surface exposed to the electrolyte corresponded to the L-LT plane at a depth of 6 mm from the top of the plate. Before the corrosion tests, the surface exposed to the electrolyte was prepared by applying an abrading procedure with 4000 grit SiC paper and a polishing procedure using 1-μm diamond paste and distilled water as the lubricant.

2.3. Mechanical behaviour

Vickers microhardness measurements were performed on a Buehler omnimet 2100 series machine with a load of 500 g. Prior to the measurements, the samples were submitted to the surface preparation procedure described for the corrosion tests. Measurements were performed on the L-LT plane. Tensile tests were carried out on a MTS mechanical tensile machine with a load cell of 30 kN. The strain rate was equal to 10^{-3} s^{-1}. The tensile samples were machined in the L direction (Fig. 1b) and were tested in the same direction. Tensile tests were performed on pre-corroded specimens without further preparation after the immersion test. Additional tests were also performed on non-corroded specimens as reference tests. In this case, prior to the mechanical tests, the tensile samples were submitted to the surface preparation procedure described for the corrosion tests. For all of the samples, microhardness measurements and tensile tests were performed in triplicate.

2.4. Characterisation of microstructure and corrosion damage

An Olympus PMG3 optical microscope (OM) was used to obtain observations of the sample surface immediately after the electrochemical measurements (OCP and current–potential curves) to characterise the corrosion damage. After exposure to the NaCl solution, the cubic samples were cut in five slices to observe the propagation of the corrosion damage in the longitudinal – short transverse (L-ST) plane (Fig. 1a). The slices were prepared according to the same procedure as that used for the preparation

of the sample prior to the corrosion tests. The slices were observed by optical microscopy, and all of the corrosion defects in the L-ST plane were detected, and their depths were measured. To ensure the relevancy of the results, two samples were analysed for each condition with five slices (1 cm length) for each sample; therefore, a 10 cm-length in the L direction (with the depth measured in the ST direction) was analysed for each condition.

The precipitation states of the different metallurgical states, *i.e.*, NHT and HT samples and samples with intermediate ageing treatments, were first characterised by transmission electron microscopy (TEM) observations using a JEOL-JEM-2010 microscope. Specifically, 300-μm slices were removed from the samples and were ground to a thickness of 100 μm. A dimple was machined in the central region using a South Bay Technology dimpler. Final electron transparency was achieved by ion milling on a precision ion polishing system (PIPS(tm), Gatan) using 5 kV Ar$^+$ ions. TEM observations were complemented by small-angle X-ray scattering (SAXS) measurements. The SAXS experiments were performed in a laboratory facility using a rotating anode at the Cu Kα wavelength (1.54 Å). The sample was ground to a thickness of approximately 70 μm and was heated in situ by a dedicated furnace, allowing for continuous measurement of the SAXS signal, which was recorded on a CCD camera. The precipitation of T_1 in the sample was identified by the apparition of scattering streaks, which were analysed in terms of the precipitate size and volume fraction using appropriate procedures. The experimental conditions and analytical procedures are described in previous reports [27,28]. To establish a relevant relationship between the distribution of T_1 precipitates and the corrosion behaviour, samples analysed by TEM and SAXS were removed at a depth of 6 mm from the top of the plate.

3. Results and discussion

3.1. Corrosion behaviour of the 2050 aluminium alloy in NHT and HT metallurgical states

Fig. 2a shows the open circuit potential (OCP) measurements performed for both NHT and HT samples in 0.7 M NaCl. The samples were immersed for 7 days, and OCP measurements were performed upon immersion in the electrolyte and after 1, 3 and 7 days

of immersion. The OCP of the NHT sample decreased slightly with an increase in the immersion time, varying from −0.615 V/SCE after 2 h in the electrolyte to −0.630 V/SCE after 7 days of immersion. In contrast, the OCP of the HT sample was essentially constant over time, varying from −0.727 V/SCE after 2 h of immersion to −0.731 V/SCE after 7 days. The observed differences in the OCP evolution over time between the two metallurgical states were attributed to the morphology of the corrosion damage that developed during immersion. OM observations of the L-LT and L-ST planes of the NHT samples after 7 days of immersion in the chloride containing solution (Figs. 2b and c, respectively) revealed intergranular corrosion damage. In contrast, for the HT sample (Figs. 2d and e), only intragranular corrosion was observed. The OCP values of the NHT sample remained less negative than those measured for the HT sample over the entire observation range (7 days). This result was in good agreement with the OCP values measured after 5 min of immersion before scanning the potential to plot the current–potential curves for both NHT and HT samples (Fig. 3a). Regardless of the metallurgical state, the global shape of the current–potential curves was the same. The cathodic region was characterised by a diffusion plateau corresponding, at least for potentials near the corrosion potential, to the reaction of oxygen reduction. Taking into account the scatter of the results, the cathodic current densities were assumed to be similar for NHT and HT samples and the corrosion current densities were between 10^{-5} A cm^{-2} and 2·10^{-5} A cm^{-2} for both NHT and HT samples. Following the corrosion potential, a sharp increase in the anodic current densities was observed for both samples which indicated that both samples were susceptible to corrosion at their corrosion potential. This result is in agreement with previous observations. The OM observations of the samples after the polarisation tests were consistent with previous observations of intergranular corrosion (Figs. 3b and c) and intragranular corrosion (Figs. 3d and e) for NHT and HT samples, respectively.

Therefore, the ageing treatment modified the corrosion susceptibility of the 2050 aluminium alloy and changed the corrosion morphology. The propagation rate of the corrosion damage was also determined, and two parameters were identified to characterise the extent of the corrosion damage in the L-ST plane, *i.e.*, the average and maximal depth of the corrosion defects. Fig. 1a shows how these parameters were determined for the two corrosion morphologies. For both NHT and HT samples, all of the corrosion defects observed for 10 slices machined in immersed samples were analysed. Thus, the analysis was performed 100 mm along the *L* direction. For all of the corrosion defects, the depth was measured perpendicularly to the L-LT plane in the ST direction, regardless of the morphology. The propagation rate was evaluated in this direction because this corresponded to the data of interest from an industrial point of view. The average depth corresponded to the arithmetic mean calculated from the depth values measured for all of the observed corrosion defects. The maximal depth corresponded to the depth of the deepest defect in the ST direction. The results obtained as a function of the immersion time in the chloride containing solution are summarised in Fig. 4. The corrosion damage propagated more rapidly in the ST direction for the NHT samples than the HT samples, which could be related to the morphology of the corrosion damage. For the HT samples, the corrosion first extended inside an entire grain and propagated in all directions. However, the corrosion mainly propagated in the *L* direction due to the grain morphology before reaching another grain. The low propagation rates observed in the ST direction after 1 day of immersion were in agreement with the proposed mechanism. Moreover, due to the relatively homogeneous size of the grains in the ST direction, the time required to corrode susceptible grains was approximately constant. This result is consistent with the fact that the average and maximal depth followed similar kinetics. Despite the low propagation rate in the ST direction, this corrosion morphology was assumed to be associated with significant weight loss due to its extent in the L-LT plane. In contrast, for the NHT samples, corrosion was localised in the grain boundaries; its extent in the L-LT plane was lower than for HT samples with a corroded surface (estimated by analysing optical observations of corroded surfaces) three times lower for NHT samples compared to HT samples, but with a more significant propagation in the ST direction. The results showed that the two corrosion morphologies corresponded to very different propagation paths. Taking into account the results from the current–potential curves, it seemed that globally (taking into account the 3 directions) the corrosion rates were not very different for NHT and HT samples but the main difference was the direction of propagation for the corrosion defects. With a preferential propagation in the L-LT plane, intragranular corrosion of HT samples was less detrimental from
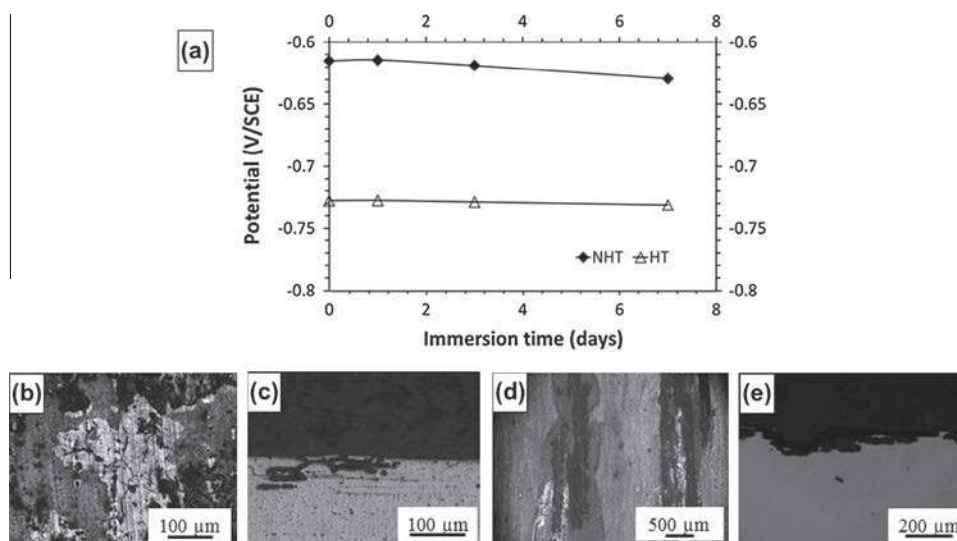
Fig. 2. (a) Open circuit potential (OCP) measurements in 0.7 M NaCl at 25 °C for the NHT and HT samples of the 2050 aluminium alloy. The surface exposed to the electrolyte was the L-LT plane. Observations of the corrosion defects in the L-LT plane (b), in the L-ST plane (c) of NHT samples, in the L-LT plane (d), in the L-ST plane (e) of HT samples. The observations were obtained using an optical microscope after 7 days of immersion in the electrolyte.
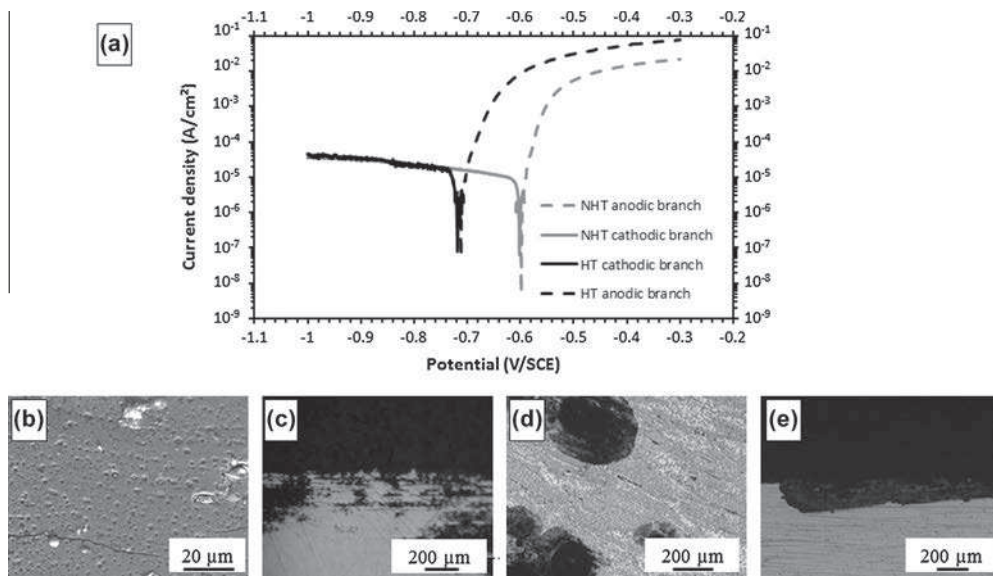
Fig. 3. (a) Current–potential curves plotted in 0.7 M NaCl at 25 °C for the NHT and HT samples of the 2050 aluminium alloy. The surface exposed to the electrolyte was the L-LT plane. Potential scan rate = 500 mV h^{-1}. Observations of the corrosion defects in the L-LT plane (b), in the L-ST plane (c) of the NHT sample, in the L-LT plane (d), in the L-ST plane (e) of the HT sample. The observations were obtained using an optical microscope after the polarisation tests.
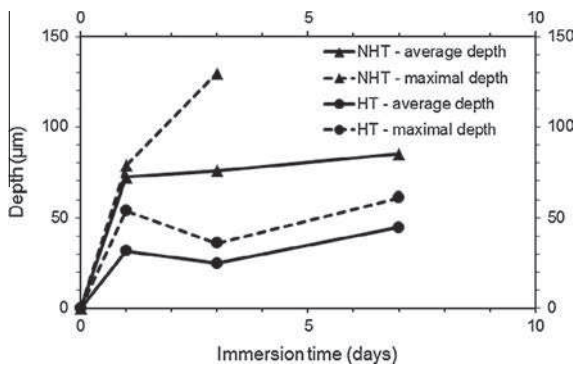
Fig. 4. Average and maximal depth of the corrosion damage versus the immersion time in 0.7 M NaCl for the NHT and HT samples.

an industrial point of view. For the NHT samples, the average depth of intergranular corrosion defects stabilised after 1 day of immersion, while the maximum depth continued to increase. This result could be explained by considering that the propagation of the intergranular corrosion damage was also promoted in the L and LT directions due to the grain morphology. However, some grains boundaries may be more reactive than others, which may lead to an increase in the maximal depth as a function of the immersion time.

Therefore, the results showed that the depth affected by corrosion was larger for NHT samples than HT samples. However, the analysis of the propagation of corrosion defects is complicated by the random nature of the corrosion compared to the size of the analysed zone: 10 slices were observed for each sample but it was probably not enough to take into account the large distribution of the corrosion defect depths. Moreover, the measurements of corrosion depth are always subjective and depend strongly on the quality of the surface preparation before the OM observations. A previous study performed on a 2024 alloy showed that it was difficult to obtain relevant data concerning the corrosion depth by analysing corroded surfaces [26]. Therefore, it was assumed that the errors on the previous corrosion depths could be significant. To obtain more relevant corrosion depth data, the method developed by Augustin

[26] was used. This method consists of determining the residual mechanical properties of pre-corroded samples. If the shape of the tensile curve for a pre-corroded sample remains unchanged compared to a reference curve for a non-corroded specimen, *i.e.,* a homothetic shift in flow stress, then one can assume that the corrosion damage is homogeneously distributed all along the gauge length and that the corroded zone can be considered a non-load bearing zone. Thus, the mean depth of the corrosion damage can be estimated by measuring the decrease in the flow stress at a given value of plastic strain. If possible, the flow stress should be measured when strain hardening is low to avoid the effects of initial crack opening phenomena. Fig. 5a and b presents the tensile curves obtained for pre-corroded NHT and HT samples, respectively, after different immersion times in 0.7 M NaCl. For the NHT samples, the strain hardening levelled off at 10% plastic strain; thus, the ultimate tensile stress (UTS) was used to determine the depth of the corroded zone. For the HT samples, little strain hardening was observed on the tensile curves; therefore, the same analysis was performed. Fig. 5c and d shows the UTS of pre-corroded NHT and HT samples, respectively, as a function of immersion times in chloride containing solutions. For the NHT samples, the UTS values decreased slightly after 1 and 3 days of exposure to a chloride containing solution. In contrast, after 7 days of immersion, a significant decrease in the UTS was observed. In the last case, the average depth of the corrosion damage was estimated to be 80 μm, which is in good agreement with the measurements previously performed by OM observations (Fig. 4) and despite the errors assumed on these data. For the HT samples, the mean depth of the corrosion damage after 7 days of immersion in 0.7 M NaCl was estimated to be 45 μm, which is also in good agreement with the previously determined values. Therefore, these results confirmed that the propagation rate of the corrosion damage in the ST direction was lower for the HT samples compared to the NHT samples. As previously stated, these results were attributed to the alloy's grain morphology and changes in the morphology of corrosion damage due to the ageing treatment.

3.2. The role of T_1 precipitates in the corrosion behaviour of the 2050 aluminium alloy

As summarised in the introduction, different studies have shown that the corrosion behaviour of Al–Cu–Li alloys is closely
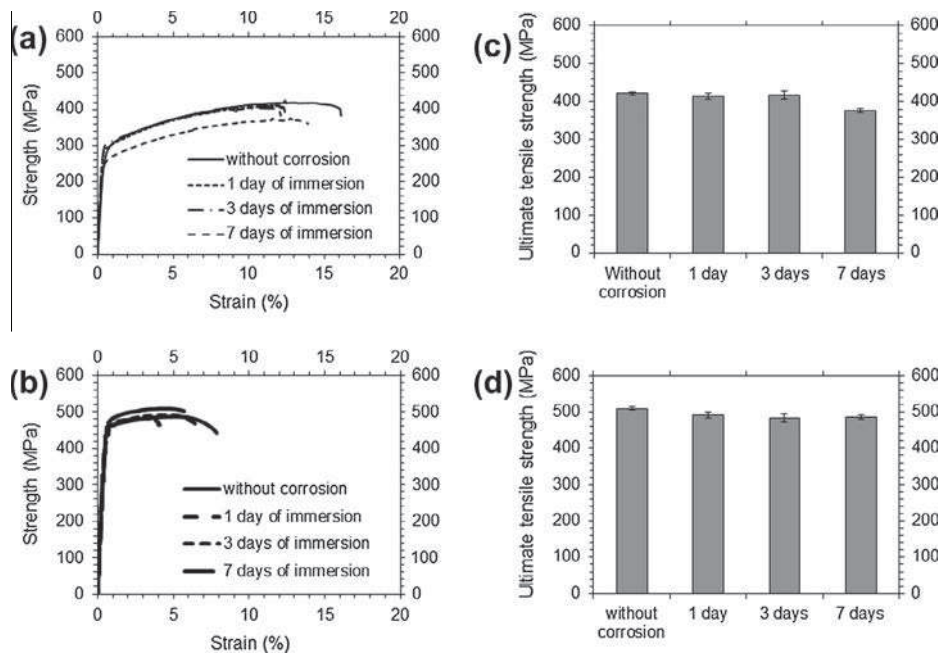
Fig. 5. Tensile curves obtained for the (a) NHT and (b) HT samples of a 2050 aluminium alloy. The curves are plotted for non-corroded samples and samples pre-corroded in 0.7 M NaCl at 25 °C for 1, 3 and 7 days. The ultimate tensile stress (UTS) versus the continuous immersion time in 0.7 M NaCl at 25 °C for (c) NHT and (d) HT samples.

linked to T_1 precipitation. Li et al. [12] found that the corrosion potential of T_1 precipitates was −1.076 V/SCE in 4% NaCl, whereas that of the matrix was equal to −0.855 V/SCE in the same solution. Therefore, galvanic coupling can occur between these precipitates and the matrix at a microscopic scale and could lead to intergranular corrosion if T_1 precipitates are present at the grain boundaries. Moreover, the presence of T_1 precipitates inside the grains could lead to a shift in the corrosion potential of the grain towards more negative values and could sensitise the grains to corrosion, leading to intragranular corrosion.

To establish the relationship between the distribution of T_1 precipitates and the corrosion behaviour for the 2050 aluminium alloy, samples aged for intermediate times (1, 2, 3, 5, 9 and 18 h) at 155 °C were subjected to additional corrosion experiments, and their microstructure and those of NHT and HT samples was analysed in parallel with TEM and SAXS measurements. Fig. 6 shows the change in the OCP in 0.7 M NaCl over time at 155 °C for the 2050 aluminium alloy and the corresponding microhardness values. The OCP decreased continuously during the ageing process. Namely, a significant decrease was observed between 0 and 9 h, followed by a slower decrease between 9 and 30 h. SAXS measurements enabled us to evaluate changes in the volume fraction of T_1 precipitates as a function of the ageing time (Fig. 7). Following a short incubation time, a rapid increase in the volume fraction was observed until a plateau was reached between 5 and 10 h of ageing. This plateau in the T_1 precipitated volume fraction was consistent with the observed plateau in the microhardness (Fig. 6). The strong increase in the microhardness in the first hours was in good agreement with the formation of intragranular T_1 precipitates, which was promoted by the ageing treatment and was consistent with the tensile results for the HT sample (Fig. 5).

In addition, TEM observations were performed for samples submitted to several ageing times (Fig. 8). The TEM micrographs obtained for the NHT sample and the samples aged for 3, 9 and 30 h (HT sample) clearly showed that the density of intragranular T_1 increased with an increase in the ageing time, which is in good agreement with the hardness values and SAXS data. The density of intragranular T_1 precipitates was estimated from the TEM
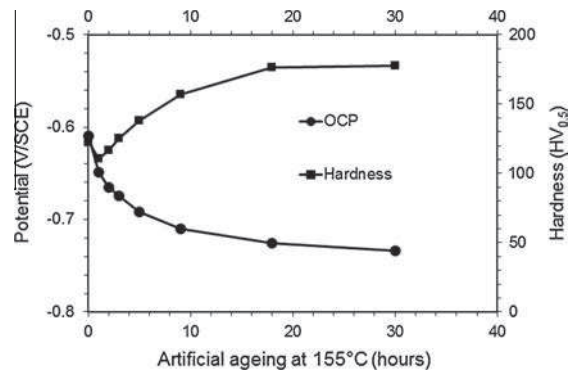
Fig. 6. Open circuit potential (OCP) measured in 0.7 M NaCl at 25 °C and Vickers hardness values (measured for a 500 g load) versus ageing time at 155 °C for the 2050-T34 aluminium alloy.
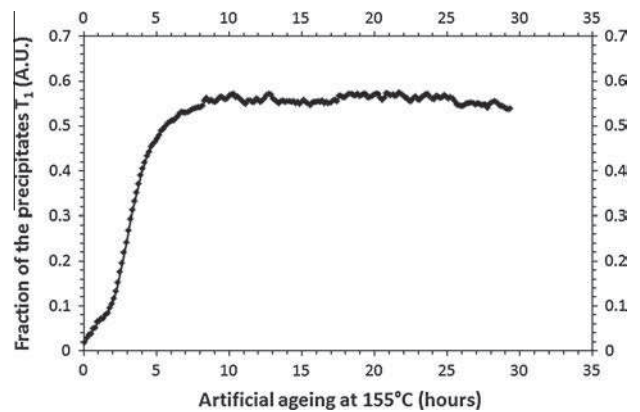
Fig. 7. Volume fraction of T_1 precipitates versus the ageing time at 155 °C for a 2050-T34 aluminium alloy (SAXS analysis).

micrographs to complete the SAXS results (Fig. 9a). More than 20 TEM micrographs were analysed for each heat treatment time.

On each micrograph, the intragranular T_1 precipitates were counted to obtain an estimate of the surface density of T_1 precipitates. By assuming that the thickness of the observed areas was constant, the surface density was considered proportional to the volume density. The results showed that the surface (volume) density of intragranular T_1 precipitates increased with an increase in the ageing time at 155 °C. The observed precipitation kinetics were in good agreement with that deduced from the hardness curve and the SAXS measurements. In addition, Fig. 9b shows that the ageing treatment also led to an increase in the size of intragranular T_1 precipitates. Intergranular precipitation was also considered in the present study. Namely, an increase in the ageing time was expected to promote the formation of T_1 precipitates or other Cu and Li containing phases such as T_2 or T_B at the grain boundaries. TEM observations showed qualitatively that the number and size of intergranular precipitates increased with an increase in the ageing time (Fig. 8). However, a quantitative characterisation of the nature of these intergranular precipitates was not carried out in the present study.

The detailed characterisation of the 2050 aluminium alloy microstructure showed that a clear correlation existed between the OCP and the presence of T_1 precipitates. This correlation mainly affects the intragranular T_1 precipitates, considering that the mechanical properties (yield and ultimate tensile stresses, hardness) were primarily dependent on the state of intragranular T_1 precipitation and that the SAXS signal was sensitive to the predom-

inant phase, i.e., the intragranular precipitates (given the large grain size of the alloy). However, it was not possible to ascertain if the OCP value was controlled by the volume fraction or size of T_1 precipitates. The ageing treatment at 155 °C led to the formation of T_1 precipitates inside the grains of the 2050 alloy, and these precipitates had a more negative corrosion potential than that of the aluminium solid solution, which led to a shift of the corrosion potential of the grain towards more negative values. Of course, the alloy may be considered a composite material consisting of grains and grain boundaries. Assuming that the surface area covered by the grain boundaries was negligible compared to that covered by the grain interiors, the corrosion potential of the alloy mainly depended on the corrosion potential of the grains. Therefore, the formation of intragranular T_1 precipitates during the ageing treatment at 155 °C led to a decrease in the OCP of the 2050 aluminium alloy. Moreover, T_1 precipitation decreased the copper content of the solid solution, which contributed to the observed reduction of the corrosion potential of the solid solution and the grain [15]. If this evolution dominated the OCP value, the observed changes were primarily dependent on the volume fraction of the T_1 precipitate.

Furthermore, significant changes in the precipitation state of the 2050 aluminium alloy were linked to the evolution of the corrosion morphology. Optical microscopy observations of the 2050 aluminium alloy samples after exposure to 0.7 M NaCl for 1 day showed that samples aged for both 3 h and 5 h were susceptible to intergranular corrosion (Fig. 10a and b), similar to the NHT
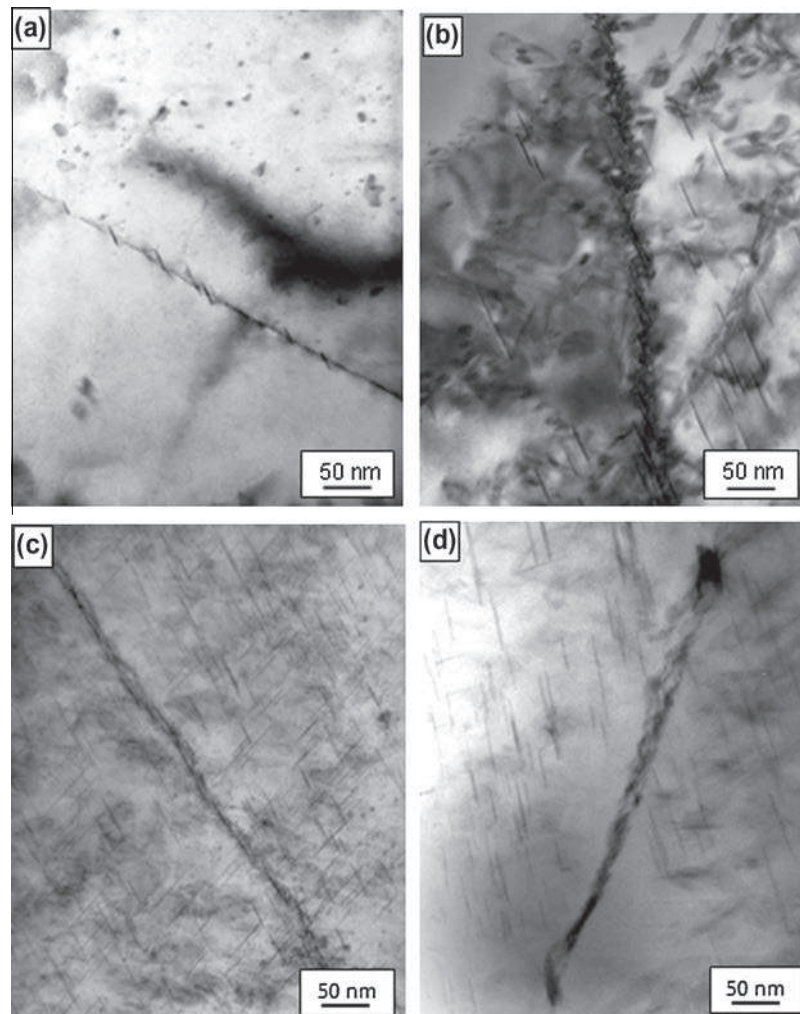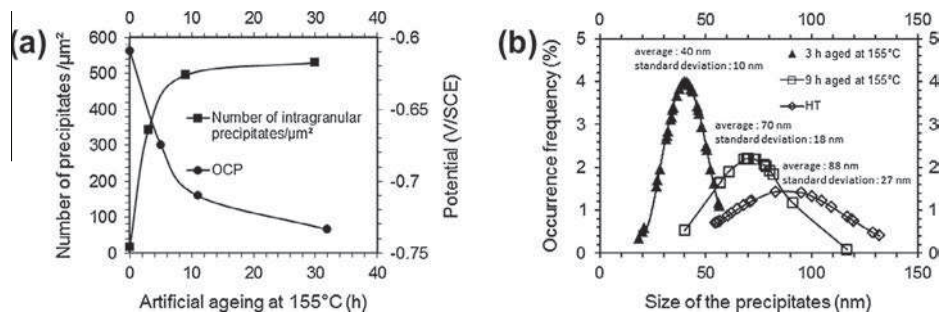

Fig. 8. TEM observations of (a) NHT (b) 2050 aluminium alloy aged for 3 h at 155 °C (c) 2050 aluminium alloy aged for 9 h at 155 °C and (d) HT samples.

Fig. 9. (a) Surface density of T_1 precipitates measured from TEM observations and the open circuit potential (OCP) measured in 0.7 M NaCl at 25 °C versus the ageing time at 155 °C. (b) Size distribution of T_1 precipitates for samples aged for 3 h at 155 °C and 9 h at 155 °C and HT samples of the 2050 aluminium alloy. Values were obtained from TEM observations. The mean size value and the standard deviation are indicated for each distribution.
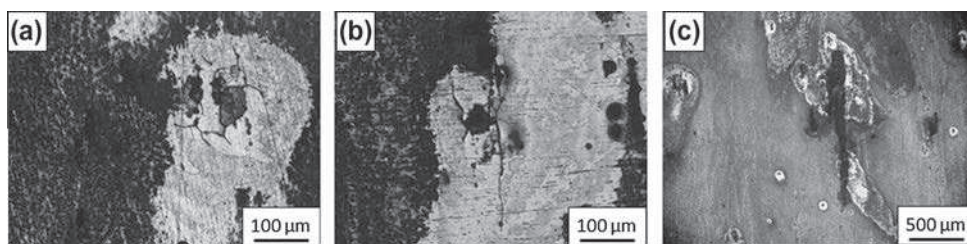
Fig. 10. Optical microscopy observations of the L-LT plane of the sample aged for (a) 3 h at 155 °C, (b) 5 h at 155 °C and (c) 9 h at 155 °C after 1 day of immersion in 0.7 M NaCl at 25 °C.
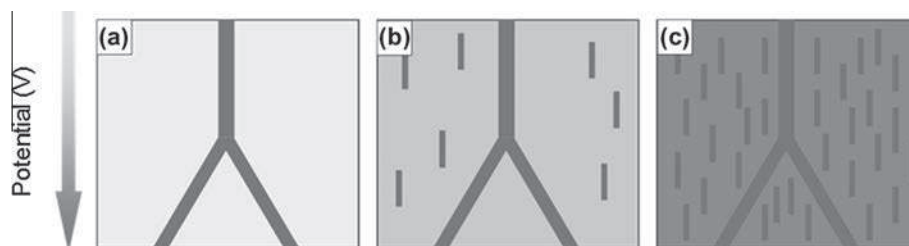
Fig. 11. Schematic representation of the electrochemical behaviour at the microstructural scale for: (a) NHT samples (b) t_1 aged samples at 155 °C with $t_1 < 9$ h, and (c) t_2 aged samples at 155 °C with $t_2 > 9$ h.

material. In contrast, the sample aged for 9 h was susceptible to intragranular corrosion (Fig. 10c), similar to the HT material. Therefore, a transition from intergranular corrosion susceptibility to intragranular corrosion susceptibility was observed during ageing at 155 °C. An ageing time of 9 h at 155 °C was critical and allowed the material to undergo the rapidly evolving stage of the T_1 precipitate microstructure.

Our results showed that the evolution of the corrosion behaviour of the 2050 aluminium alloy during the ageing treatment can be explained by considering the distribution of both intergranular and intragranular T_1 precipitates. Fig. 11 is a schematic representation of the distribution of T_1 precipitates as a function of the ageing treatment. In this figure, the grey level of the microstructural elements (precipitates and solid solution) was indicative of the electrochemical behaviour of the elements. As the corrosion potential of the elements became more negative, the grey colour became more intense. The NHT sample was characterised by T_1 precipitates-free grains separated by grain boundaries decorated by a few precipitates that may be of the T_1 phase (Fig. 11a). Due to the rather negative corrosion potential of T_1 precipitates compared to that of the solid solution, the entire grain boundary acts as a sacrificial anode, leading to a strong susceptibility of the alloy

to intergranular corrosion. When the 2050 aluminium alloy was aged at 155 °C, the size and density of intergranular precipitates increased (Fig. 11b), which could led to a more negative corrosion potential for the grain boundaries. At the same time, intragranular T_1 precipitation occurred. This precipitation phenomenon combined with a reduction of the copper content in the solid solution led to a shift of the corrosion potential of the grain towards more negative values. Therefore, the entire material showed stronger anodic behaviour when the ageing time increased due to the redistribution of alloying elements. This result is consistent with the OCP (Fig. 2) values measured for HT samples, as well as the OCP versus ageing time (Fig. 6). However, for times shorter than 9 h, the difference in the corrosion potential between the grains and grain boundaries was sufficiently high, and grain boundaries were less noble than the grains, causing the alloy to be susceptible to intergranular corrosion. Lastly, when the ageing time was longer than 9 h, the fraction of intragranular T_1 precipitates was sufficient, and the corrosion potential of the grains shifted towards negative values. Thus, the difference in electrochemical behaviour between the grains and grain boundaries was reduced to a level where galvanic coupling did not occur, which enhanced the material's susceptibility to intragranular corrosion. Moreover, due to their

negative corrosion potential, the grains became intrinsically more susceptible to corrosion, which is consistent with this corrosion morphology. The latter corrosion morphology was less detrimental for the material. As a result, the 2050-T34 alloy aged at 155 °C was more resistant to corrosion than the 2050-T34 alloy.

4. Conclusions

The corrosion behaviour of the recently developed Al–Cu–Li 2050 alloy was studied in a chloride containing solution. In the T34 metallurgical state (NHT), the alloy was susceptible to intergranular corrosion. During the course of ageing at 155 °C, the alloy became progressively susceptible to intragranular corrosion, which is a less detrimental corrosion morphology for aerospace applications. On the basis of corrosion tests, mechanical properties measurements, TEM observations and SAXS measurements, we established a clear correlation between the corrosion behaviour and the precipitation of the T_1 phase. The results showed that the ageing treatment resulted in the formation and growth of both intergranular precipitates and intragranular T_1 precipitates, which decreased the copper content in solid solution. Therefore, as a result of ageing, the electrochemical behaviour of the grains and grain boundaries was homogenised, which explains the evolution of the corrosion morphology.

Acknowledgments

References

[1] C. Meric, Physical and mechanical properties of cast under vacuum aluminum alloy 2024 containing lithium additions, Mater. Res. Bull. 35 (2000) 1479–1494.

[2] Ph. Lequeu, R. Muzzolini, J. C. Ehrstrom, F. Bron, R. Maziarz, High-Performance Friction Stir Welded Structures Using Advanced Alloys, Aeromat conference, Seattle, WA, 2006.

[3] R.J. Rioja, J. Liu, The evolution of Al–Li base products for aerospace and space applications, Metall. Mater. Trans. A 43A (2012) 3325–3337.

[4] B.-P. Huang, Z.-Q. Zheng, Effects of Li content on precipitation in Al–Cu–(Li)–Mg–Ag–Zr alloys, Scr. Mater. 38 (1998) 357–362.

[5] B. Decreus, A. Deschamps, F. De Geuser, P. Donnadieu, C. Sigli, M. Weyland, The influence of Cu/Li ratio on precipitation in Al–Cu–Li–x alloys, Acta Mater. 61 (2013) 2207–2218.

[6] W.A. Cassada, G.J. Shiflet, E.A. Starke Jr., Mechanism of Al$_2$CuLi (T_1) nucleation and growth, Metall. Mater. Trans. A 22A (1991) 287–297.

[7] W.A. Cassada, G.J. Shiflet, E.A. Starke Jr., The effect of plastic deformation on Al$_2$CuLi (T_1) precipitation, Metall. Mater. Trans. A 22A (1991) 299–306.

[8] B.M. Gable, A.W. Zhu, A.A. Csontos, E.A. Starke Jr., The role of plastic deformation on the competitive microstructural evolution and mechanical properties of a novel Al–Li–Cu–X alloy, J. Light Met. 1 (2001) 1–14.

[9] P.S. Chen, B.N. Bhat, Time–Temperature–Precipitation Behavior in Al–Li Alloy 2195, NASA/TM 2002–211548, 2002.

[10] H. Li, Y. Tang, Z. Zeng, Z. Zheng, F. Zheng, Effect of ageing time on strength and microstructures of an Al–Cu–Li–Zn–Mg–Mn–Zr alloy, Mater. Sci. Eng. A 498 (2008) 314–320.

[11] J.F. Li, C.X. Li, Z.W. Peng, W.J. Chen, Z.Q. Zheng, Corrosion mechanism associated with T_1 and T_2 precipitates of Al–Cu–Li alloys in NaCl solution, J. Alloys Compd. 460 (2008) 688–693.

[12] J.F. Li, Z.Q. Zheng, W.D. Ren, W.J. Chen, X.S. Zhao, S.C. Li, Simulation on function mechanism of T_1(Al$_2$CuLi) precipitate in localized corrosion of Al–Cu–Li alloys, Trans. Nonferrous Met. Soc. China 16 (2006) 1268–1273.

[13] R.G. Buchheit, J.P. Moran, G.E. Stoner, Electrochemical behavior of the T_1 (Al$_2$CuLi) intermetallic compound and its role in localized corrosion of Al–2% Li–3% Cu Alloys, Corrosion 50 (1994) 120–130.

[14] V. Proton, J. Alexis, E. Andrieu, J. Delfosse, M.-C. Laffont, C. Blanc, Characterization and understanding of the corrosion behaviour of the nugget in a 2050 aluminium alloy friction stir welding joint, Corros. Sci. 73 (2013) 130–142.

[15] C. Henon, S. Rouault, Comparison of corrosion performance and mechanisms of Al–Cu alloys with and without Li addition, in: Proceeding of the 13th International Conference on aluminium alloys, TMS, Pittsburgh, USA, June 3–7 2012.

[16] H.Y. Li, Y. Tang, Z.D. Zeng, F. Zheng, Exfoliation corrosion of T6- and T8-aged Al$_x$Cu$_y$Li$_z$ alloy, Trans. Nonferrous Met. Soc. China 18 (2008) 778–783.

[17] J.E. Kertz, P.I. Gouma, R.G. Buccheit, Localized corrosion susceptibility of Al–Li–Cu–Mg–Zn alloy AF/C458 due to interrupted quenching from solutionizing temperatures, Metall. Mater. Trans. A 32A (2001) 2561–2573.

[18] J.P. Moran, F.S. Bovard, J.D. Chrzan, R.J. Rioja, E.L. Colvin, Improvements in corrosion resistance offered by newer generation 2x99 aluminium–lithium alloy for aerospace applications, in: Proceeding of the 12th International Conference on Aluminium alloys, Yokohama, Japon, September 5–9, 2010.

[19] N. Jiang, J.F. Li, Z.Q. Zheng, Trans. Nonferrous Met. Soc. China 15 (2005) 23–29.

[20] K.D. Ralston, D. Fabijanic, N. Birbilis, Effect of grain size on corrosion of high purity aluminium, Electrochim. Acta 56 (2011) 1729–1736.

[21] K.D. Ralston, N. Birbilis, C.H.J. Davies, Revealing the relationship between grain size and corrosion rate of metals, Scripta Mater. 63 (2010) 1201–1204.

[22] J.G. Brunner, N. Birbilis, K.D. Ralston, S. Virtanen, Impact of ultrafine-grained microstructure on the corrosion of aluminium alloy AA2024, Corros. Sci. 57 (2012) 209–214.

[23] S. Gollapudi, Grain size distribution effects on the corrosion behaviour of materials, Corros. Sci. 62 (2012) 90–94.

[24] S. Zhao, D.A. Wolfe, T.S. Huang, G.S. Frankel, Generalized model for IGC growth in aluminum alloys, J. Statist. Plann. Inference 137 (2007) 2405–2412.

[25] T.S. Mahmoud, Effect of friction stir processing on electrical conductivity and corrosion resistance of AA6063-T6 Al alloy, J. Mech. Eng. Sci. 222 (2008) 1117–1123.

[26] C. Augustin, E. Andrieu, C. Blanc, J. Delfosse, G. Odemer, Empirical propagation laws of intergranular corrosion defects affecting 2024 T351 alloy in chloride solutions, J. Electrochem. Soc. 157 (2010) C428–C436.

[27] F. De Geuser, F. Bley, A. Deschamps, A new method for evaluating the size of plate-like precipitates by small-angle scattering, J. Appl. Cryst. 45 (2012) 1208–1218.

[28] A. Deschamps, F. De Geuser, Quantitative characterization of precipitate microstructures in metallic alloys using small-angle scattering, Metall. Mater. Trans. A 44A (2013) 77–85.